Gas-Liquid Two-phase Stratified Flow Interface Reconstruction with Sparse Batch Normalization Convolutional Neural Network

Gas-Liquid Two-phase Stratified Flow Interface Reconstruction with Sparse Batch Normalization Convolutional Neural Network

Chao Tan, *Senior Member, IEEE,* Feng Li, Shuhua Lv, Yunjie Yang *Member, IEEE* and Feng Dong, *Senior Member, IEEE*

***Abstract*— Two-phase stratified flow is ubiquitous in industrial processes, monitoring its phase interface is important for improving the safety and efficiency of process. Electrical Resistance Tomography is a promising non-intrusive visualization technique for monitoring two-phase flow. However, some electrodes could lose their contact with the liquid in stratified flow, aggravating the under-determined image reconstruction solution and resulting in low-quality reconstructed image in traditional methods. In this paper, a sparse batch normalization convolutional neural network (SBN-CNN) method is proposed for accurate and rapid gas-liquid interface reconstruction. Up-sampling and normalization were used for preprocessing of measurements. A novel network structure including convolution, pooling and batch normalization layers was designed to extract features from sparse measurements and the images were reconstructed by deep fully connected layers. After batch-based training, the proposed SBN-CNN achieves a superior performance to the-state-of-art methods in terms of convergence rate, imaging accuracy, noise resistance and generalization ability, through experimental validation.**

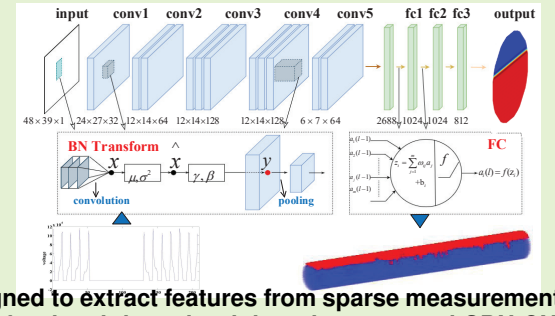

***Index Terms*— Gas-Liquid Stratified Flow, Electrical Resistance Tomography, Interface Reconstruction, Batch Normalization, Convolutional Neural Network**

I. Introduction

TWO-phase stratified flow is ubiquitous in industrial production process, e.g. pneumatic conveyance of granular solids, long-distance transportation of hydrocarbons, interfacial heat and mass transfer [1]. Online monitoring the transit interface of two-phase flow is important to improve the safety and efficiency of industrial production, which requires a measurement technology be fast enough to capture the transient change and also easy to be implemented in the pipeline. Electrical Resistance Tomography (ERT) is a non-intrusive process visualization technique with the advantages of low cost, radiation-free and high speed [2]. It can be used to reconstruct the dynamic interface of two fluids with different conductivity.

An ERT sensor consists of a set of electrodes evenly mounted around the periphery of the pipe. The boundary voltage measurements are obtained by subsequently injecting electric currents into one selected pair of electrodes and measuring voltages from the others. The reconstruction of conductivity distribution with boundary voltage data is a typical nonlinear, under-determined and ill-posed inverse problem [3]. If the excitation or measurement electrodes are in contact with non-conductive fluid, the corresponding measurements will be invalid and the number of effective measurements will decrease, which aggravates the under-determined issue of the image reconstruction problem. Unlike in other flow regimes, the phenomenon of invalid measurements is particularly common in gas-liquid two-phase stratified flow [4], therefore it is very difficult to reconstruct the interface with traditional image reconstruction algorithms.

To address this problem, many studies have been done to mitigate the aggravated under-determined problem resulted from invalid electrodes [5], [6]. Ma *et al.* extracted a common feature in the voltage data when some electrodes are in contact with gas [7]. They put forward a liquid level detection method which can identify whether a water surface exists in the measured field and find out its position. However, this method can only recognize 14 special water surface positions including the full pipe state. Babaeizadeh *et al.* proposed a boundary element method (BEM) [8], which converts the original problem of reconstructing the domain's conductivity distribution into estimating the subdomains' boundaries. Ren

This work was supported by the National Natural Science Foundation of China, No. 61973229.

Chao Tan, Feng Li, Shuhua Lv and Feng Dong are with the Tianjin Key Laboratory of Process Measurement and Control, School of Electrical and Information Engineering, Tianjin University, Tianjin 300072, China. e-mail: tanchao@tju.edu.cn, fengli@tju.edu.cn, lvshuhua@tju.edu.cn, fdong@tju.edu.cn

Yunjie Yang is with Institute for Digital Communications, School of Engineering, The University of Edinburgh, Edinburgh, UK. e-mail: y.yang@ed.ac.uk

Manuscript received Feb xx, 2021.

et al. presented a physical model of ERT for interface reconstruction by using BEM and solved the inverse problem using the Levenberg-Marquardt method [9]. Although BEM methods obtained good results, there are two weaknesses. Firstly, their conclusions are all drawn with a correct prior knowledge of the water's conductivity. If the prior information deviates from its true value, the estimated results deteriorate. Secondly, to obtain accurate estimation, it requires the number of effective electrodes to be larger than five. Decreasing the number of effective electrodes will significantly reduce the estimation quality.

Among the reported results for interface reconstruction of two-phase stratified flow, there are mainly three disadvantages. First, in most studies only interfaces at specific locations of the pipe have been discussed, which limited their applications. Second, as accurate as possible prior information is required in some iterative image reconstruction algorithms, and their solving processes are time-consuming and usually of low precision. Third, no dynamic experimental results are reported in most of the research. In conclusion, influenced by invalid electrodes, it is a big challenge to realize accurate reconstruction from relatively fewer measurements. Therefore, a novel theoretical framework is needed to solve such problems.

Recently, deep learning has generated an overwhelming enthusiasm in several imaging applications [10], [11]. It can efficiently learn high-level features from data through a hierarchical network framework [12]. Several deep learning algorithms have been proposed for image reconstruction of electrical tomography using different network models [13]–[16]. Jin *et al.* established a benchmark dataset for Electrical Capacitance Tomography and put forward a deep autoencoder-based iteration method to evaluate reconstruction results on this database [13]. Lei *et al.* proposed a Deep Extreme Learning Machine (DELM) method to ameliorate the reconstruction accuracy [15]. The DELM combined with split Bregman (SB) method and fast iterative shrinkage thresholding (FIST) algorithm realized competitive reconstruction both on numerical and experimental data. Li *et al.* presented a deep neural network combined with stacked autoencoder and logistic regression to improve the quality of reconstruction in Electrical Impedance Tomography [16]. However, most of such studies focus on the image reconstruction of different inclusions, and in such cases all the electrodes are in contact with conductive fluid. Considering the existence of invalid electrodes, the effective measurements obtained by ERT sensors become far less than the unknowns to be solved in gas-liquid stratified flow, which deteriorates the under-determined image reconstruction problem. To tackle this problem, some special improvement and design are required to be made under the basic deep learning framework, in order to adapt it to interface reconstruction.

In this work, a novel sparse batch normalization convolutional neural network (SBN-CNN) structure is proposed by exploiting the characteristics of the measurements. The input nodes of the network are sparse measurements as most of the invalid measurements are zero. A hierarchy of convolution and pooling is used to extract high-level features from low-dimension and sparse measurements. Batch Normalization [17] is designed between the convolutional and the pooling layers to solve the problem of slow updating speed of parameters caused by the sparse measurements, which consequently reduces the error of interface reconstruction. An improved gradient-based optimization method, i.e. Adam [18] with temporal averaging, which can adjust the update step size adaptively and overstep the local optimum, is used to minimize the distance between the network output and the true conductivity distribution. The proposed SBN-CNN adopts data-driven method, which can automatically search the optimal solution in the solution space without introducing prior knowledge. The reduction of effective measurements is compensated by the designed efficient feature extraction layers, which have strong data representation ability even on sparse measurements.

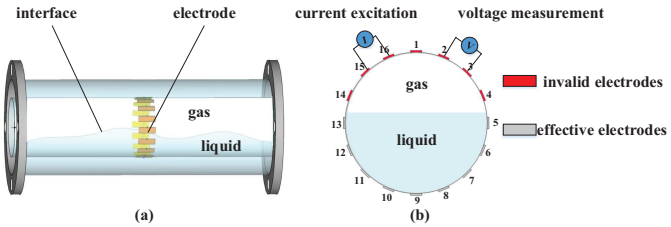

Fig. 1: Measurement setup of stratified flow with ERT. (a) horizontal pipe with ERT sensors, (b) interface distribution in cross-section.

II. INTERFACE RECONSTRUCTION WITH SBN-CNN

A. Stratified Flow Reconstruction with ERT

The 16-electrode adjacent excitation mode is usually adopted in ERT [19]. The electric potential distribution ϕ , conductivity σ and excitation current I satisfy the Laplace equation, which can be formulated as:

$$\begin{cases} \nabla \cdot (\sigma \nabla \phi) = 0 \\ \int\limits_{E^+} \sigma \cdot \frac{\partial \phi}{\partial n} ds = +I \\ \int\limits_{E-} \sigma \cdot \frac{\partial \phi}{\partial n} ds = -I \end{cases} \tag{1}$$

where n is boundary exterior normal vector; E is electric field intensity. The measurement setup of gas-liquid two-phase stratified flow in a horizontal pipe is shown in Fig. 1. When the excitation electrodes are covered by non-conductive gas, the sensitive field cannot be established in the measured field. As a result, the corresponding measurements will be zero. These measurements are invalid because they do not contain effective information reflecting the conductivity distribution of fluid. If all electrodes are in contact with conductive fluid, according to the reciprocity theorem, there will be $N(N-3)/2$ effective measurement data, where N is the number of electrodes. However, there are only $(N_v-2)(N_v-3)/2$ effective measurements in measuring stratified flow [7], where N_v is the number of valid electrodes and $N_v \leq N$. It should be aware that the reduction of the number of effective data aggravates the under-determined problem in image reconstruction.

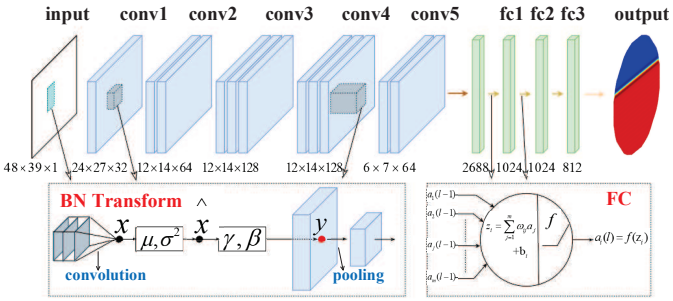

Fig. 2: Structure of SBN-CNN

B. Sparse Batch Normalization Convolutional Neural Network

Deep CNNs can automate the learning of features from sparse measurements by utilizing a large database of samples. The output of CNN is then fed into a deep fully connected neural network (FCN), which aims to map a set of 2-D features into a series of labels for each input. Finally, all the labels are padded into the measured field to generate the fluid distribution.

It is essential to define a CNN-based strategy for extracting features automatically from sparse measurement data and use those features for accurately interface reconstruction from both the training database and also from an independent set of test measurements. Based on the sparse characteristics of the measurement data, the overall architecture of the proposed SBN-CNN is shown in Fig. 2. The network includes 5 convolutional (conv1 to conv5) layers to hierarchically mapping the original sparse measurements to multiple feature maps and 3 fully connected (fc1 to fc3) layers to integrate the information of multiple feature maps to the final fluid distribution. Batch normalization is applied to the input, conv1 and conv4 layer in a convolutional way to alleviate the problem of slow parameters updating speed caused by sparse data.

To address the problem of sparse measurement data, interface reconstruction by SBN-CNN involves the following five basic stages: (1) data acquisition, (2) preprocessing, (3) feature extraction, (4) image reconstruction and (5) model selection and training, as shown in Fig. 3.

1) Data acquisition: There are 106750 samples generated in the training dataset by solving the forward problem through simulation, which are divided into 4 different types of interfaces. As demonstrated in Fig. 4, case 1 shows the measurement when the interface is near invalid electrodes, case 2 represents the interface near effective electrodes, case 3 represents the interface in the middle of invalid electrodes and effective electrodes, and case 4 represents the interface in the middle of the same electrodes. To make the simulation interface closer to the real dynamic experiment interface, there are horizontal, declining and wave interfaces in each case, and the number of each interface type is approximately equal. In the simulation models with different interface types, the number of invalid electrodes is different, and the measurement of effective electrodes is affected by the interface type.

2) Preprocessing: Due to system noise and the large range of measurement, it is necessary to preprocess the ERT boundary measurement information before inputting them into the SBN-CNN [20]. To avoid the instability of the imaging result caused by the fluctuation of the measurement with the system noise, ERT measurement is processed as follows:

$$u = u_g - u_w \tag{2}$$

where, u_g is the boundary voltage vector with objects in the sensing area, while u_w is the boundary voltage vector when the field is full of water, u is the difference vector between u_g and u_w. To simplify the description, u is collectively referred to as boundary measurement voltage vector, and is normalized in the dataset as follows:

$$\hat{u}_i = \frac{\|u_i - min(u)\|}{\|max(u) - min(u)\|} \tag{3}$$

where, u_i is the ith element of u, $\hat{u}_i$ is the normalized value of u_i. Measurement vectors before and after preprocessing are shown in Fig. 5.

The original measurement of ERT is a vector after preprocessing, while the inputs of CNNs are 2-D matrix, the first step is to convert vectors to a 2-D matrix. Each row in the matrix represents the measured data under one excitation. To alleviate the problem of dimension disappearance caused by pooling operation without losing effective information, up-sampling operation is implemented by padding the same measurement data around the original matrix.

3) Feature extraction: CNNs can automatically learn features from (typically massive) databases and have a good generalization ability [21]. From this perspective, 5 convolutional layers are used to extract useful features from sparse measurements. The dimension of input matrix is $48 \times 39 \times 1$, which is 3 times of the original matrix due to up-sampling operation as illustrated above. The conv1 uses 1×13 kernel to learn the features of measurements under one excitation, so it can summarize the statistical characteristics of measurement data at different invalid electrodes. Other convolution layers adopt 3×3 kernels to extract local features under different excitation and the pooling layers adopt 2×2 kernels for feature reduction. It is observed in the experiments that the activation values of invalid measurement data are close to zero when the network becomes deeper, which results in a small gradient of back propagation and a low parameters updating speed. Therefore, batch normalization is applied to accelerate the training speed of feature extraction. It accomplishes this by normalizing layer inputs with means and variances and has a beneficial effect on the gradient flow through the network by reducing the dependence of gradients on initial values. Meanwhile, as a regularization method, batch normalization can avoid overfitting. In such case, the original convolutional output $y = f(Wa + b)$ is replaced with $y = f(BN(Wa))$ by BN transform, where W and b are learned parameters of the model, f is the ReLU nonlinearity. For a feature map $x = Wa$ and a mini-batch B$=\{x_{1,2\cdots m}\}$, according to [17],

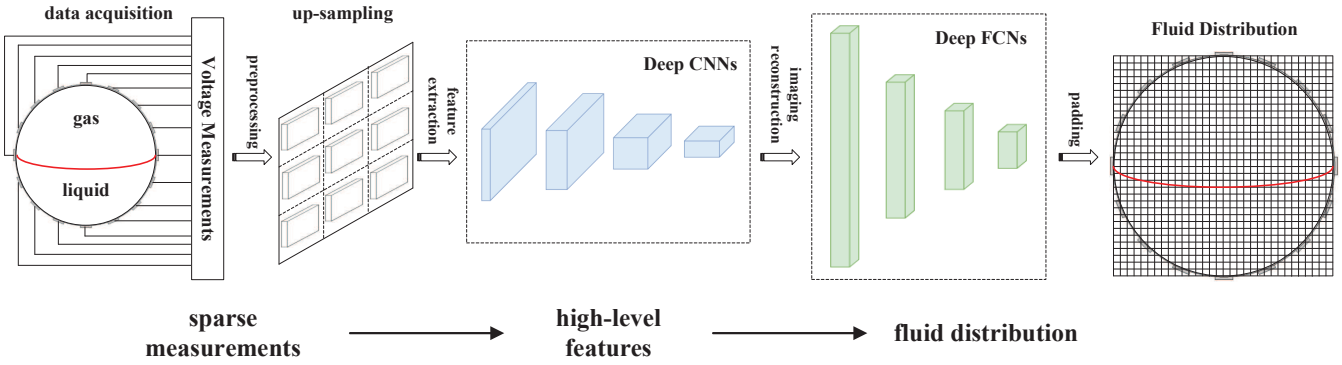

Fig. 3: Interface reconstruction process with SBN-CNN

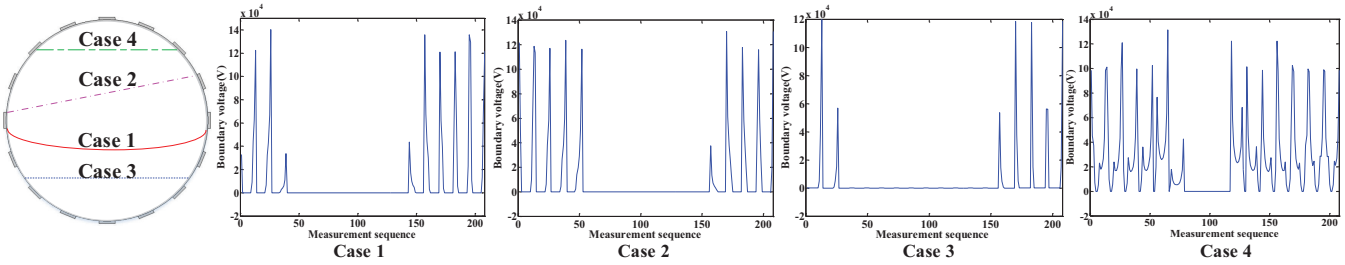

Fig. 4: Different types of interface in the training dataset

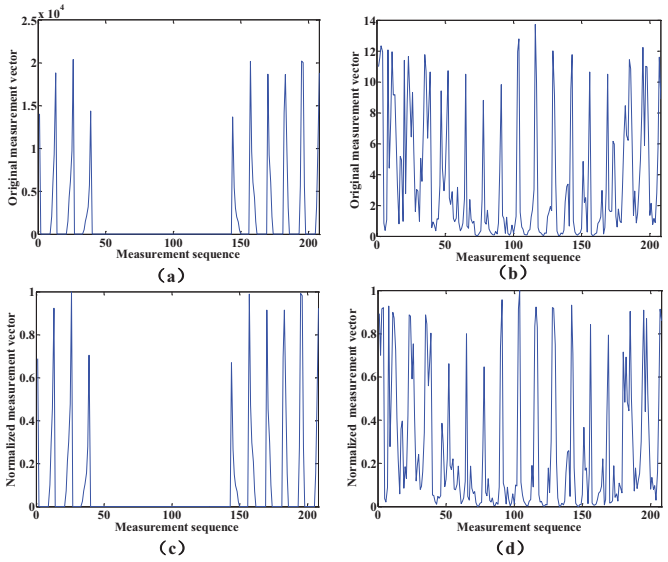

Fig. 5: Measurement vector. (a) original measurement vector of simulation, (b) original measurement vector of dynamic experiment, (c) normalized measurement vector of simulation, (d) normalized measurement vector of dynamic experiment.

the parameters in BN transform are defined as:

$$\mu_{\mathrm{B}}=\frac{1}{m}\sum_{i=1}^{m}x_i \tag{4}$$

$$\sigma_{\mathrm{B}}^2=\frac{1}{m}\sum_{i=1}^{m}(x_i-\mu_{\mathrm{B}})^2 \tag{5}$$

$$\hat{x_i}=\frac{x_i-\mu_{\mathrm{B}}}{\sqrt{\sigma_{\mathrm{B}}^2+\varepsilon}} \tag{6}$$

$$y_i=\gamma\hat{x_i}+\beta \tag{7}$$

4) Interface reconstruction: FCNs are used to accomplish the course of interface reconstruction from the output maps of the last stage of CNNs. Because the output volume of a CNN consists of 2-D maps and the inputs to FCNs are vectors, the first step is to convert 2-D arrays to vectors. Then the computation performed by the FC frame in Fig. 4 is:

$$a_i(l)=f(\sum_{j=1}^{n_{l-1}}w_{ij}(l)a_j(l-1)+b_i(l)) \tag{8}$$

where $w_{ij}(l)$ is the weight of the ith neuron in layer l, which associates that neuron with the output of the jth neuron in layer $l-1$; $a_j(l-1)$ is the output of the jth neuron in layer $l-1$; $b_i(l)$ is the bias of the ith neuron in layer l; n_{l-1} is the number of neurons in layer $l-1$; f denotes nonlinearity. ReLU nonlinearity is used in the fc1 and fc2 layer, but softmax regression is applied before the final nonlinearity to turn the output of the neural network into a probability distribution, which is convenient to compute cross entropy loss. Finally, the output of fc3 is padded into a circle region to accomplish the interface reconstruction.

5) Model selection and training: two different state-of-the-art networks were compared with the proposed SBN-CNN, including FC (fully connection neural network with only a hidden layer) and CNN2 [14]. The Relative Image Error (RIE) and Image Correlation Coefficient (ICC), which are defined in (7) and (8) respectively, are chosen for quantitative assessment

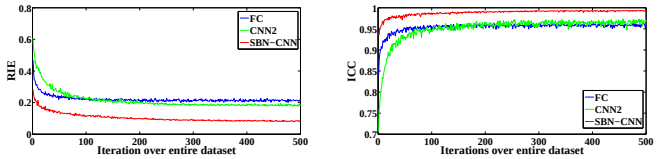

Fig. 6: RIE and ICC during training with different networks

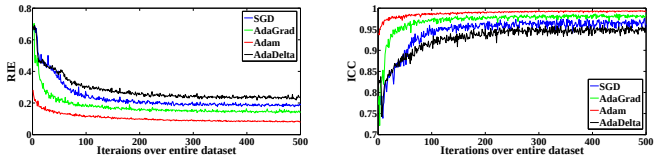

Fig. 7: RIE and ICC during training with different optimization method

of reconstruction quality:

$$RIE = \frac{\left\|\hat{Y} - Y\right\|}{\|Y\|} \tag{9}$$

$$ICC = \frac{\sum_{i=1}^{N}(\hat{Y}_i - \bar{\hat{Y}})(Y_i - \bar{Y})}{\sqrt{\sum_{i=1}^{N}(\hat{Y}_i - \bar{\hat{Y}})^2 \sum_{i=1}^{N}(Y_i - \bar{Y})^2}} \tag{10}$$

where Y is the real distribution, $\hat{Y}$ is the reconstruct distribution, $\hat{Y}_i$ is the ith element of $\hat{Y}$, $\bar{\hat{Y}}$ is the mean of $\hat{Y}$, Y_i is the ith element of Y, $\bar{Y}$ is the mean of Y. The change of RIE and ICC during training with different networks is shown in Fig. 6. It can be seen that the proposed model produced a large margin in RIE and ICC and converged more rapidly.

To make the training more effective, four different stochastic gradient-based optimization methods, i.e. stochastic gradient descent (SGD) [22], AdaGrad [23], AdaDelta and Adam with temporal averaging, were tested using the same network structure. The results are in Fig. 7. Adam with temporal averaging shows marginal improvement over others both in convergence speed and reconstruction quality. Different from the original Adam in [18], temporal averaging of parameters θ is added for a better generalization performance since the last iteration is noisy due to stochastic approximation. So the final update rule is $\bar{\theta}_t = \beta_2 \cdot \bar{\theta}_{t-1} + (1 - \beta_2)\theta_t$ on the basis of Adam algorithm, where β_2 is decay rate that gives a higher weight to more recent parameter values.

When training with batch normalization, a training example is seen in conjunction with other examples in the mini-batch. So the training network no longer produces deterministic values for a given training example. It is advantageous to the generalization of the network as the Dropout [24] does. However, it will offset each other when batch normalization and dropout were used in the same network, as shown in Fig. 8, where CNN5 represents the same network as SBN-CNN but without batch normalization. It can be seen that there is no significant improvement when batch normalization and

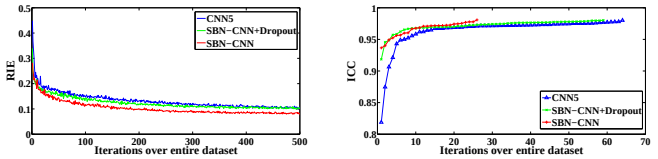

Fig. 8: RIE and ICC during training with batch normalization variants

dropout are both applied. While removing dropout in SBN-CNN model can speed up training and reduce RIE further. Therefore, the SBN-CNN model without dropout is adopted as the final structure. In this research, after 7 hours of training, the imaging speed of SBN-CNN is about 5 ms/image.

III. EXPERIMENTAL DESIGN AND RESULTS

The proposed SBN-CNN model is trained with simulation data and validated with both simulation and experimental data. It was compared with two state-of-the-art methods in terms of reconstruction accuracy and noise reduction. The diameter of the pipeline in experiment is different from that in simulation, which is used to evaluate its generalization ability in practice.

A. Simulation Results

Simulated data were obtained by solving the forward problem with finite element method. The conductivity of the water and gas is set to 0.04 $S \cdot m^{-1}$ and 1e-6 $S \cdot m^{-1}$ respectively. In the simulation test, the gas-liquid interface near the invalid electrode and the effective electrode are studied, the reconstruction results are shown in Fig. 9, where 3, 5, 7and 9 represent the number of invalid electrodes.

Two widely studied algorithms for ERT image reconstruction, i.e. total variation (TV) regularization algorithm [25] and CNN2 method [14], are used for reconstruction performance comparison. TV algorithm has better characteristic on stability and edge preservation. To make it suitable for interface reconstruction in stratified flow, some preprocessing has been performed in measurement data. First, the locations of all invalid electrodes are determined based on sparse measurement data according to [7]. Then the abnormal measurement data caused by invalid electrodes are removed from all measurements. Finally, the conductivity is reconstructed based on the remaining valid measurements, which is called TV-effective data method. It can be seen in Fig. 9 that TV-effective data method suffered from serious artifacts and the interface reconstructed was generally lower than the ground truth particularly in Case 1. The interface reconstructed by CNN2 method was closer to the ground truth than TV, but the interface was fuzzy and there were artifacts inside the liquid phase. SBN-CNN method reconstructed a more accurate interface and eliminated most artifacts than other methods. The quantitative results of the three method for different simulation models in Fig. 9 are listed in Table. I, SBN-CNN method obtained the best scores on most cases.

The proposed method was also evaluated in terms of noise suppression performance. Fig. 10 presents the results with

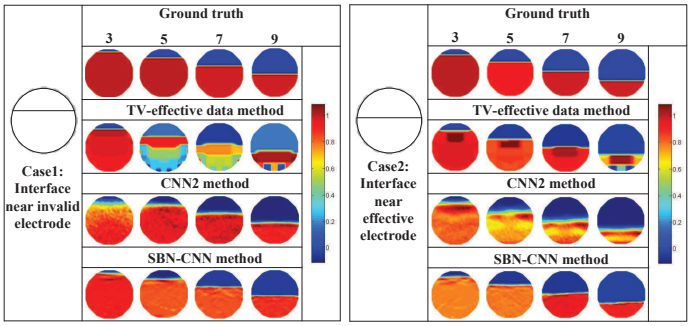

Fig. 9: Reconstructed images of two different interface distribution

TABLE I: QUANTITATIVE RESULTS ASSOCIATED WITH DIFFERENT ALGORITHMS FOR INTERFACE RECONSTRUCTION

Case 1	Algorithm	RIE	ICC
3	TV-effective data	23.5%	0.644
	CNN2	15.1%	0.641
	SBN-CNN	**6.3%**	**0.944**
5	TV-effective data	57.5%	0.603
	CNN2	10.9%	0.976
	SBN-CNN	**6.2%**	**0.988**
7	TV-effective data	53.4%	0.915
	CNN2	13.9%	0.991
	SBN-CNN	**4.7%**	**0.997**
9	TV-effective data	50.6%	0.941
	CNN2	18.1%	0.977
	SBN-CNN	**4.9%**	**0.998**

Case 2	Algorithm	RIE	ICC
3	TV-effective data	20.9%	0.881
	CNN2	11.9%	0.930
	SBN-CNN	**6.0%**	**0.981**
5	TV-effective data	29.5%	0.961
	CNN2	18.4%	0.964
	SBN-CNN	**10.2%**	**0.996**
7	TV-effective data	15.2%	**0.995**
	CNN2	22.1%	0.961
	SBN-CNN	**13.0%**	0.992
9	TV-effective data	46.6%	0.928
	CNN2	25.4%	0.953
	SBN-CNN	**16.5%**	**0.983**

three different noise levels, i.e. white Gaussian noise with signal-to-noise ratio of 5, 10 and 15 dB respectively. It can be observed that SBN-CNN can effectively restrain white Gaussian noise with a signal-to-noise ratio of 15 dB. There are certain deviations when white Gaussian noise with signal-to-noise ratio of 5 and 10 dB are added to the measurements. But the ICCs are no less than 0.85 in most of the cases. Table. II gives the mean measurements (average $\pm$ standard deviation) for all the six different types of interfaces. It can be seen that the proposed SBN-CNN is robust for certain magnitude of noise. The comparison of anti-noise performance between SBN-CNN and CNN2 is shown in Fig. 11. It shows the change

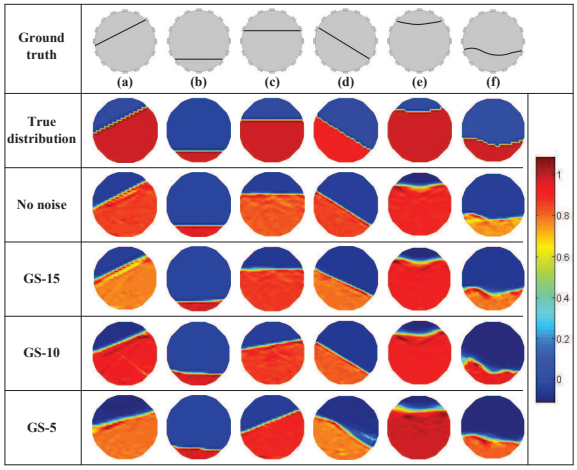

Fig. 10: Reconstructed images with different noise

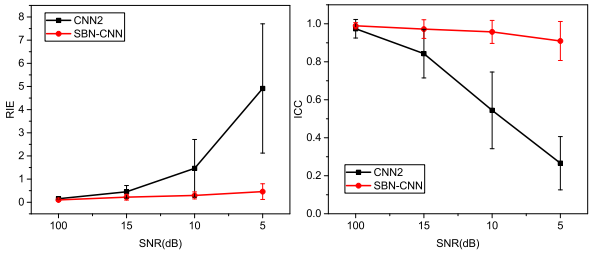

Fig. 11: The comparison of anti-noise performance between SBN-CNN and CNN2

of RIE and ICC mean and standard deviations with the change of noise level. The quality of image reconstruction using CNN2 deteriorates sharply with the increase of noise level. In contrast, the reconstruction quality of SBN-CNN changes smoothly, proving that the proposed model is more robust to noise.

B. Experimental Results

Both static and dynamic experiments were conducted to evaluate the performance of the proposed SBN-CNN. Fig. 12 shows the high-speed ERT system, including a data acquisition system, a pipe section with a 16-electrode sensor and the data collection software. In this experiment, the excitation current is a sinusoidal signal with an amplitude of 2.5 mA and a frequency of 50KHz. The diameter and length of the horizontal pipe are 100 mm and 220 mm respectively. The length, width and thickness of the electrodes are 30mm, 10mm and 1mm respectively. The conductivity of tap water and gas in horizontal pipe is about 0.04 $S \cdot m^{-1}$ and 0 $S \cdot m^{-1}$. Different interface heights were tested by injecting various volumes of water into the horizontal pipe. The reconstruction results are given in Fig. 13. The first and forth rows are the actual interface height. The second and fifth rows show the relative position of the interface height to the electrodes. The third and six rows denote the reconstruction results with the proposed SBN-CNN. It can be seen that the proposed method can give accurate height regardless of the type of interfaces in most of

TABLE II: QUANTITATIVE RESULTS(MEAN ± SDs) ASSOCIATED WITH DIFFERENT NOISES FOR INTERFACE RECONSTRUCTION

Noise level		No noise	GS_15	GS_10	GS_5
(a)	RIE	0.10 ± 0.04	0.22 ± 0.12	0.30 ± 0.15	0.47 ± 0.34
	ICC	0.99 ± 0.02	0.97 ± 0.04	0.96 ± 0.06	0.91 ± 0.11
(b)	RIE	0.08 ± 0.06	0.25 ± 0.18	0.32 ± 0.20	0.47 ± 0.24
	ICC	0.99 ± 0.02	0.95 ± 0.08	0.93 ± 0.09	0.87 ± 0.13
(c)	RIE	0.15 ± 0.16	0.28 ± 0.19	0.42 ± 0.31	0.50 ± 0.23
	ICC	0.95 ± 0.10	0.91 ± 0.18	0.84 ± 0.24	0.81 ± 0.20
(d)	RIE	0.10 ± 0.03	0.22 ± 0.13	0.30 ± 0.15	0.46 ± 0.34
	ICC	0.99 ± 0.02	0.97 ± 0.05	0.96 ± 0.06	0.91 ± 0.10
(e)	RIE	0.18 ± 0.10	0.31 ± 0.19	0.35 ± 0.19	0.47 ± 0.24
	ICC	0.96 ± 0.04	0.93 ± 0.07	0.91 ± 0.08	0.87 ± 0.10
(f)	RIE	0.19 ± 0.11	0.32 ± 0.19	0.37 ± 0.21	0.49 ± 0.28
	ICC	0.96 ± 0.04	0.93 ± 0.08	0.90 ± 0.09	0.86 ± 0.11

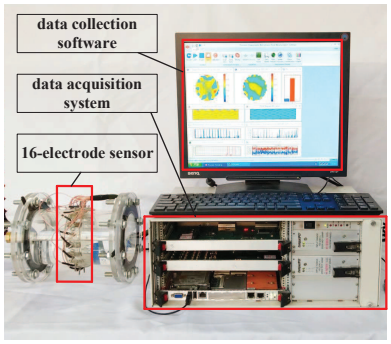

Fig. 12: The ERT system for experimental investigation

the cases. Table. III summarizes the quantitative results from the eight images. In addition to the two criteria, i.e. RIE and ICC, height error is also used to measure the reconstruction accuracy, which is defined as:

$$height\ error = h_r - h_t \tag{11}$$

where h_r stands for the reconstruction height from the conductivity distribution, h_t is the true height obtained from the first and third lines in Fig. 13. Although a few interfaces have larger RIE, all the ICCs are no less than 0.9 and the mean value of height errors is 1.9 mm. This means that the SBN-CNN has good robustness and generalization ability to some extent. In order to further examine the effectiveness of the proposed method, dynamic experiments were also carried out.

Dynamic experiments were conducted on a multiphase flow loop as shown in Fig. 14. The diameter of the pipeline is 50mm. Gas was pumped into the pipeline through a desiccator after a filter and an air compressor. The water and gas are mixed by a T-mixer. Before mixing, the volume flow rate of each phase is controlled by adjusting valve and measured by standard single-phase flowmeter. A 16-electrode sensor was installed in the pipeline. In the experiments, different heights of interfaces were produced by changing the flow rate of single-phase fluid of either gas or water.

In order to obtain the complete and stable flow characteristics of each experimental condition, the continuous test of each flow state last for 10 seconds. Table. IV gives the

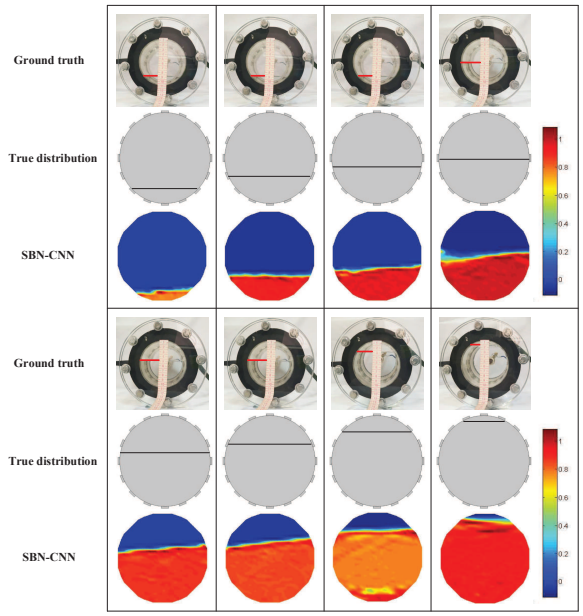

Fig. 13: The interface reconstruction results in static experiment

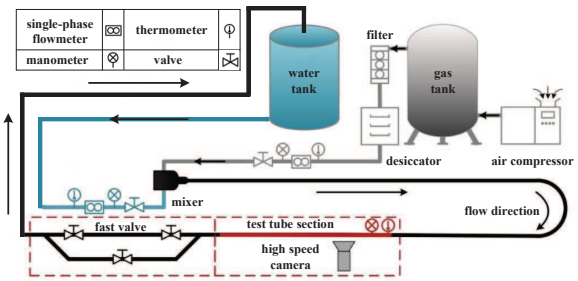

Fig. 14: Experimental rig for multiphase flow

corresponding parameters in different experimental conditions. The SBN-CNN imaging results of typical time slice under 625 frames/second of ERT data acquisition speed are shown in Fig. 15. The first column shows the flow state obtained by a high speed camera. Although the reconstructed image contains

TABLE III: QUANTITATIVE RESULTS IN STATIC EXPERIMENT

Water content (%)	11.76	23.53	35.29	47.06	58.82	70.59	82.35	94.12
Interface height (mm)	16.0	27.0	37.5	47.5	56.0	66.0	77.5	89.7
RIE	0.60	0.15	0.15	0.22	0.19	0.18	0.11	0.08
ICC	0.90	0.99	0.99	0.98	0.97	0.96	0.98	0.91
height error (mm)	-4.23	-0.65	-0.73	2.76	3.04	2.29	0.82	-0.74

TABLE IV: THE EXPERIMENT CONDITIONS IN DYNAMIC EXPERIMENTS

Model	Gas Velocity (m/s)	Liquid Velocity (m/s)
(a)	0.18	0.23
(b)	2.87	0.04
(c)	0.05	0.15

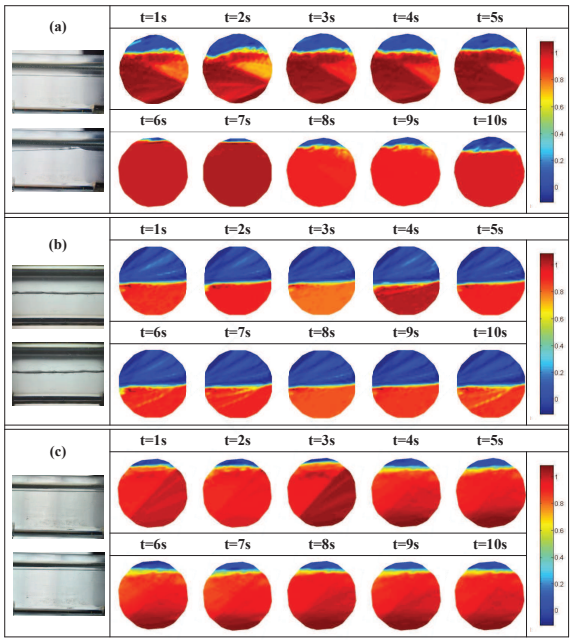

Fig. 15: The image reconstruction results in dynamic experiment

Fig. 16: Multi-images flowing the same cross-section at different times

some artifacts, there are still clear interface consistent with the true distribution. In model (a), it can be seen that the interface height changes significantly at 6 seconds and gradually recovers from 8 seconds. In order to display the change of interface height more intuitively, multi-images flowing the same cross-section at different times are stacked to form a 3D image, which are shown in Fig. 16. It illustrates that the proposed SBN-CNN method is effective even on complex dynamic flow conditions.

IV. Conclusion

When ERT is used to measure gas-liquid two-phase stratified flow in horizontal pipes, the failure of some electrodes due to gas coverage will severely affect the reconstruction of interface distribution. In view of this problem, a data-driven method based on CNN is proposed. The complete procedure is divided into four steps, i.e. data acquisition, preprocessing, feature extraction and image reconstruction. Four different types of interface are simulated by solving the forward problem in ERT. Normalization and up-sampling of measurement data are used as noise reduction and geometric corrections. A hierarchical CNN structure combined with batch normalization is designed to extract high-level features from low-dimension and sparse measurements. Batch normalization that normalizes layer inputs by mean and variance can alleviate the problem of slow parameter update speed caused by sparse data. The interface reconstruction is finally accomplished by three fully connected layers, which can map several feature maps to interface distribution. An improved stochastic gradient descent method, i.e. Adam with temporal averaging, was presented to accelerate convergence speed and enhance reconstruction accuracy. The numerical simulation results have demonstrated a higher ICC and lower RIE than some state-of-the-art methods both on visual observations and quantitative evaluation. It is proved that the model has good anti-noise performance by adding different levels of noise to the measurements. Both static and dynamic experiments have validated that the model has a good generalization ability. In the future, more attempts will be made to further improve the performance of the model on experimental data and extend it to 3D reconstruction.

References

[1] X. W. Shi, C. Tan, H. Wu, and F. Dong, An Electrical and Ultrasonic Doppler System for Industrial Multiphase Flow Measurement, *IEEE Transactions on Instrumentation and Measurement* vol. 70, p. 9154454, 2021, doi: 10.1109/tim.2020.3013080.

[2] F. Li, C. Tan, F. Dong, *et al.*, V-Net Deep Imaging Method for Electrical Resistance Tomography. *IEEE Sensors Journal*, vol. 20, no. 12, pp. p. 6460-6469, 2020

[3] M. Wang, Industrial Tomography: Systems and Applications (Electronic and Optical Materials, no. 71). Cambridge: Woodhead Publishing, 2015.

[4] M. Wang, W. Yin, and N. Holliday, A highly adaptive electrical impedance sensing system for flow measurement, *Measurement Science and Technology*. vol. 13, no. 12, pp. 1884-1889, 2002.

[5] B. S. Kim, A. K. Khambampati, S. Kim, *et al.*, Image reconstruction with an adaptive threshold technique in electrical resistance tomography, *Measurement Science and Technology*. vol. 22, no. 10, pp. 104009, 2011.

[6] B. S. Kim, A. K. Khambampati, Y. J. Hong, *et al.*, Multiphase flow imaging using an adaptive multi-threshold technique in electrical resistance tomography, *Flow Measurement and Instrumentation*. vol. 31, pp. 25-34, 2013.

[7] Y. X. Ma, Z. C. Zheng, L. A. Xu, *et al.*, Application of electrical resistance tomography system to monitor gas/liquid two-phase flow in a horizontal pipe, *Flow Measurement and Instrumentation*. vol. 12, no. 4, pp. 259-265, 2001.

[8] S. Babaeizadeh, D. H. Brooks, D. Isaacson, *et al.*, Electrode boundary conditions and experimental validation for BEM-based EIT forward and inverse solutions, *IEEE Transactions on Medical Imaging*. vol. 25, no. 9, pp. 1180-1188, 2006.

[9] S. J. Ren, F. Dong, C. Tan, and Y. Y. Xu, A boundary element approach to estimate the free surface in stratified two-phase flow, *Measurement Science and Technology*. vol. 23, no. 10, pp. 105401, 2012.

[10] X. P. Jiang, J. Sun, C. H. Li, *et al.*, Video image defogging recognition based on recurrent neural network, *IEEE Transactions on Industrial Informatics*. vol. 14, no. 7, pp. 3281-3288, 2018.

[11] N. Lv, C. Chen, T. Qiu, *et al.*, Deep learning and superpixel feature extraction based on contractive autoencoder for change detection in SAR images, *IEEE Transactions on Industrial Informatics*. vol. 14, no. 12, pp. 5530-5538, 2018.

[12] Y. LeCun, Y. Bengio, and G. Hinton, Deep learning, *Nature*. vol. 521, pp. 436-444, 2015.

[13] J. Zheng, J. K. Li, Y. Li, *et al.*, A benchmark dataset and deep learning-based image reconstruction for electrical capacitance tomography, *Sensors (Basel, Switzerland)*. vol. 18, no. 11, pp. 18113701, 2018.

[14] C. Tan, S. H. Lv, F. Dong, *et al.*, Image reconstruction based on convolutional neural network for electrical resistance tomography, *IEEE Sensors Journal*. vol. 19, no. 1, pp. 196-204, 2019.

[15] J. Lei, Q. B. Liu, and X. Y. Wang, Deep learning-based inversion method for imaging problems in electrical capacitance tomography, *IEEE Transactions on Instrumentation and Measurement*. pp. 2107-2118, 2018.

[16] X. Y. Li, Y. Lu, J. M. Wang, *et al.*, An image reconstruction framework based on deep neural network for electrical impedance tomography, *IEEE International Conference on Image Processing (ICIP)*. pp. 3585-3589, 2017.

[17] S. Ioffe, and C. Szegedy, Batch normalization: accelerating deep network training by reducing internal covariate shift, *International Conference on*. pp. 448-456, 2015.

[18] P. K. Diederik, and L. B. Jimmy, ADAM: A method for stochastic optimization, *Computer Science*. 2014.

[19] Y. Y. Xu, F. Dong, ang C. Tan, Electrical resistance tomography for locating inclusions using analytical boundary element integrals and their partial derivatives, *Engineering Analysis with Boundary Elements*. vol. 34, pp. 876-883, 2010.

[20] R. C. Gonzalez, Deep convolutional neural networks, *IEEE Signal Processing Magazine*. vol. 35, no. 6, pp. 79-87, 2018.

[21] P. Li, Z. K. Chen, L. T. Yang, *et al.*, Deep convolutional computation model for feature learning on big data in internet of things, *IEEE Transactions on Industrial Informatics*. vol. 14, no. 2, pp. 790-798, Feb. 2018.

[22] G. E. Hinton, and R. R. Salakhutdinov, Reducing the dimensionality of data with neural networks, *Science*. vol. 313, no. 5786, pp. 504-507, 2006.

[23] D. John, H. Elad and S. Yoram, Adaptive subgradient methods for online learning and stochastic optimization, *Machine Learning Research*. vol. 12, pp. 2121-2159, 2011.

[24] N. Srivastava, G. Hinton, A. Krizhevsky, *et al.*, Dropout: A simple way to prevent neural networks from overfitting, *Journal of Machine Learning Research*. vol. 15, no. 1, pp. 1929-1958, 2014.

[25] X. Z. Song, Y. B. Xu, and F. Dong, A spatially adaptive total variation regularization method for electrical resistance tomography, *Measurement Science and Technology*. vol. 26, no. 12, pp. 125401, 2015.